FLUORESCING AEROSOLS AND CLOUDS: INVESTIGATIONS OF CO-EXISTENCE

Jens Reichardt[1,*], **Ronny Leinweber**[1] **and Anne Schwebe**[1]

[1]*Richard-Aßmann-Observatorium, Deutscher Wetterdienst, Am Observatorium 12, 15848 Lindenberg, Germany,* [*]*jens.reichardt@dwd.de*

ABSTRACT

RAMSES of the Lindenberg Meteorological Observatory, Germany, is the first multipurpose lidar to routinely measure the fluorescence spectra of atmospheric aerosols. Combined with the other measurement parameters (cloud water content and optical properties, moisture and temperature), this capability allows one to study the co-existence of clouds and fluorescing aerosols for the first time. The fluorescence receiver is briefly described, and measurement examples are presented and discussed.

1 INTRODUCTION

Its scientific relevance notwithstanding, lidar studies of cloud-aerosol co-existence and, prospectively, interaction have not been attempted so far because conventional elastic-backscatter or Raman lidars cannot distinguish between scattering from different particles, and so the aerosol signal is masked in the presence of clouds. With its new fluorescence spectrometer, the spectroscopic Raman lidar RAMSES [1, 2] is the first instrument to make such a distinction: Pure condensed water does not fluoresce while experience shows aerosols in the vast majority of cases do. So fluorescence observed within clouds unveils the occurrence of aerosol particles. In this contribution the integration of the fluorescence spectrometer into the RAMSES instrument is outlined. Furthermore, aerosol observations are discussed, particularly with regard to the interdependence between aerosol type, spectral characteristics and source region; and with regard to the co-existence of aerosols and clouds.

2 FLUORESCENCE SPECTROMETER

Similarly to the water spectrometer [2], the fluorescence spectrometer has been added to the RAMSES far-range receiver. Like the former, it consists of four main components, (1) the fiber coupler which images the atmospheric return signals transmitted by a dichroic beamsplitter used to suppress visible light in the vibrational-rotational Raman detection channels (BS7, see Fig. 4(b) of [1]) onto the circular front face (2.3-mm diameter) of a, (2) quartz/quartz fiber bundle (100-μm cores, 0.12 numerical aperture). The fiber bundle, rectangularly reshaped, is coupled into a, (3) 1/8-m grating spectrograph (600 grooves per millimeter, 500-nm blaze). In its focal plane a, (4) 32-channel multianode photomultiplier single-photon-counting detection system is mounted (SP32-20, Licel GmbH, Berlin, Germany), yielding a spectral resolution of about 12.8 nm per detection channel. The wavelength range of the spectrometer covers the near UV and the visible light spectrum, however, because of the spectral characteristics of the above-mentioned beamsplitter, fluorescence spectra are only attainable > 440 nm. Fortunately, the transmitted signal of the 387-nm Raman band of molecular nitrogen is sufficiently strong to be used for spectrum calibration. As a first step, relative calibration of the spectrum measurement is obtained by inserting a light source of known spectral characteristics into the telescope hall and illuminating the far-range receiver field stop. An absolute calibration is then achieved by comparing measured and calculated (from spectroscopic and concurrent radiosonde data) molecular-nitrogen Raman signals. Light extinction by particles and molecules is taken into account.

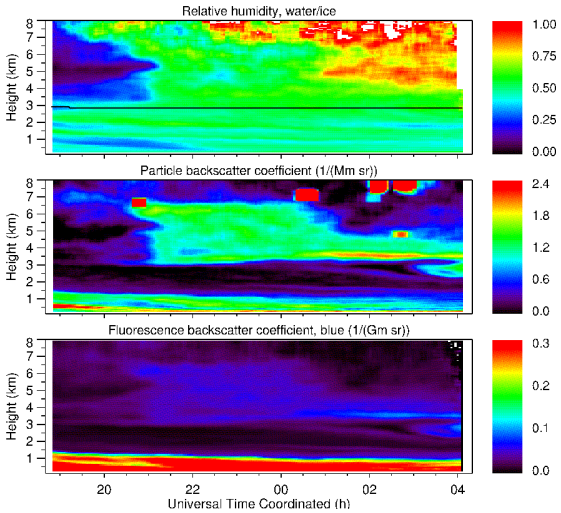

Figure 1: Temporal evolution of relative humidity (with respect to liquid water and ice above and below 0°C, respectively; 0°C-isotherm indicated by black curve), particle backscatter coefficient, and fluorescence backscatter coefficient (455–530 nm spectral range) as measured with RAMSES during the night of 2–3 April 2016. Whitened stretches indicate times and heights where data did not pass quality control.

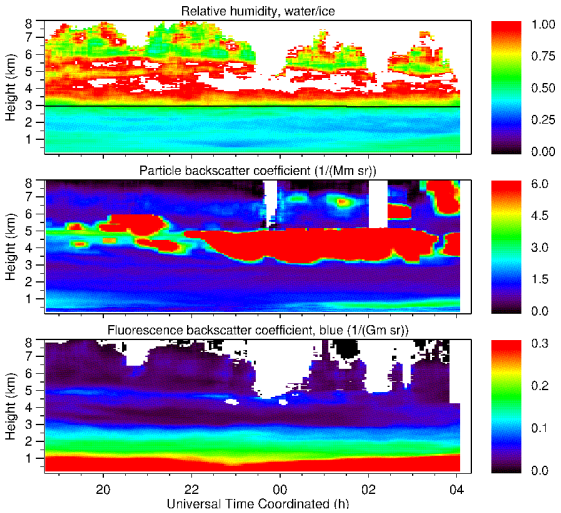

Figure 2: Similar to Fig. 1 but for the night of 3–4 April 2016.

3 MEASUREMENT EXAMPLES

3.1 Saharan dust

As a first measurement example, the Saharan dust event in early April 2016 is presented in Figs. 1–3. RAMSES was operating continuously, but only nighttime measurements are discussed when data from the fluorescence spectrometer are available. Figure 1 depicts the advent of the dust plume which originated from Algeria and Mali according to simulations with the FLEXPART Lagrangian particle dispersion model [3]. Fluorescence is low, and, with a spectral maximum missing > 440 nm, the spectrum resembles those usually observed for boundary-layer aerosols under unperturbed conditions (see Fig. 7). Optical properties are homogeneous. Particle depolarization ratios, δ_{par}, of about 30–35%, and lidar ratios, S_{par}, between 60 and 80 sr (not shown) indicate particle diameters of about 0.8 μm, according to finite-difference time-domain scattering computations [4] for quartz-rich irregular aerosol particles with an aspect ratio of 1. A short-lived change in particle properties to values typical of ice clouds ($\delta_{\mathrm{par}} = 15\%$, $S_{\mathrm{par}} = 25$ sr) is observed at the leading edge of the aerosol plume at 20:45 UTC (Fig. 1), but the elastic backscatter coefficient, β_{par}, is rather small ($\sim 3.5\,\mathrm{Mm^{-1}sr^{-1}}$), and the relative humidity with respect to ice, RHi, low (about 60%). Similar events occur at later times and slightly higher altitudes at much higher RHi values. Note that sporadic cirrus clouds were present above 9 km. The strong fluorescence below 1.5 km is indicative of a polluted boundary layer.

The next day, a mostly frozen cloud appeared in a moistened layer between 3.5 and 5.5 km. Interestingly, obscured by elastic cloud scattering otherwise, the fluorescence measurement reveals the presence of the weakly-fluorescing dust aerosol in the cloud-top layer (Fig. 2). Origin and spectral characteristics of the aerosol are very similar to what was found the day before. As an example of a combined measurement of elastic and fluorescence cloud and aerosol properties, Fig. 3 shows the RAMSES observation at 22 UTC. RHi hardly reaches ice saturation within the cloud, elastic-backscatter

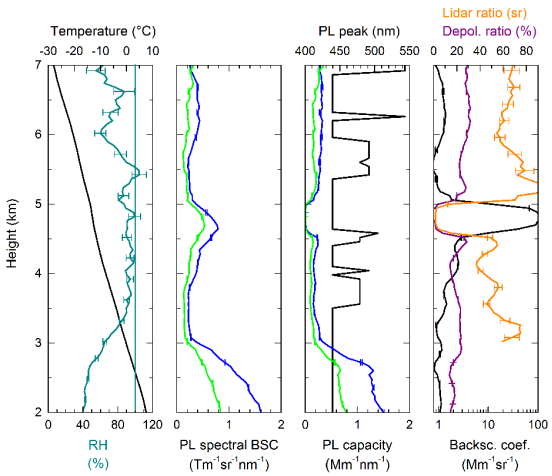

Figure 3: Relative humidity with respect to ice, and temperature (interpolated; from 6-hourly radiosonde data); mean green (540–615 nm spectral range) and blue (455–530 nm) fluorescence spectral backscatter coefficients; green and blue fluorescence capacities (mean fluorescence spectral backscatter coefficient divided by particle backscatter coefficient), and wavelength of spectral maximum; and particle backscatter coefficient, and depolarization and lidar ratios as measured on 3 April 2016 at 22 UTC. Bars indicate statistical errors of the lidar measurement. Note the logarithmic scale of the elastic backscatter coefficient.

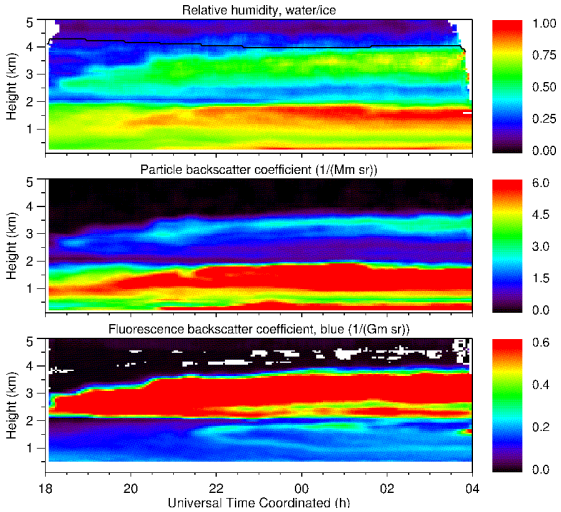

Figure 4: Similar to Fig. 1 but for the night of 9–10 September 2016.

peak and fluorescence spectral backscatter coefficient maxima roughly coincide in height. Cloud optical properties are characteristic of horizontally aligned ice particles. Note that fluorescence capacity is several times larger below 3 km, which suggests differences in aerosol composition even though the fluorescence spectra (not shown) in the wavelength range currently accessible with RAMSES is similar.

3.2 Biomass-burning aerosol (BBA)

On 9 September 2016 aerosols from Africa were measured in the lower free troposphere (2–3.7 km; ($\delta_{\mathrm{par}} < 10\%$, $S_{\mathrm{par}} = 60$ sr)) again (Fig. 4), but the source region was slightly more to the southwest. Interestingly, the fluorescence properties differ vastly from those of the Apr 2016 cases: The aerosol fluoresces much more strongly (e.g., blue fluorescence capacity of about 5–7 $\mathrm{Mm^{-1}nm^{-1}}$ as compared to $\leq 1\,\mathrm{Mm^{-1}nm^{-1}}$), and the spectrum exhibits a distinct local maximum at 490–500 nm (Fig. 7). This may indicate the presence of BBA because fluorescence spectra of local Easter bonfires show a similar peak, albeit at longer wavelengths (Fig. 7). Relative humidity with respect to liquid water, RHw, is between 35% and 80%, β_{par} correlates with RHw, but humidity is insufficient for cloud formation.

Hardly visible in Fig. 4, but yet confirmed by a Lindenberg in-situ optical backscatter sonde launched at 23 UTC, is another BBA layer at heights around 5 km. It is remnant of a larger BBA event that could be observed for several days starting on 6 September 2016 (Fig. 5). While β_{par} is near the detection limit, the BBA shows a brilliant fluorescence display. The spectrum closely resembles the spectrum measured near the ground during the bonfires. The air masses of the vertically well-defined layer were advected from North America, very dry ($< 20\%$ RHi) and thus void of clouds. Incidentally, a thin cirrus was observed aloft (> 9 km) during the whole night.

Finally, Fig. 6 illustrates a BBA incident dur-

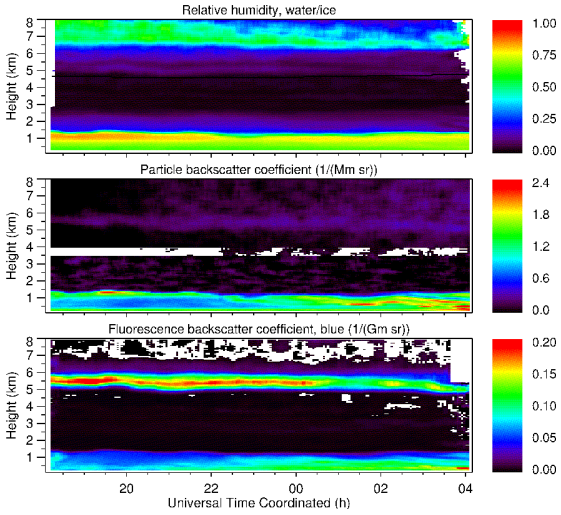

Figure 5: Similar to Fig. 1 but for the night of 6–7 September 2016.

ing which cirrus clouds occurred. The measurement was taken in the night of 7–8 September 2015, note the fine fluorescence streaks. A remarkable observation is that the descending cloud-top layer is strongly correlated with a BBA filament. Unfortunately, data quality is insufficient to determine RHi within the cirrus.

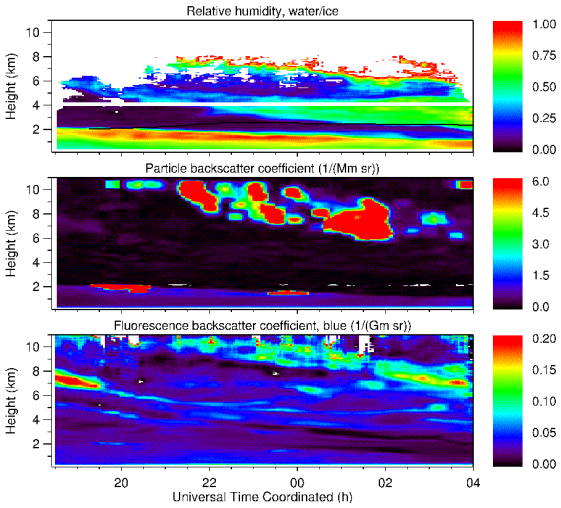

Figure 6: Similar to Fig. 1 but for the night of 7–8 September 2015.

In conclusion, the fluorescence spectrometer has proven to be a promising tool to study aerosol-cloud co-existence. The information extracted from the fluorescence spectra is sufficient to allow for a rough aerosol classification, which is an important result per se because backtrajectory calculations are often inconclusive and not meaningful enough to determine aerosol type. Experimental work is underway to extend measurements of the fluorescence spectrum to wavelengths < 440 nm.

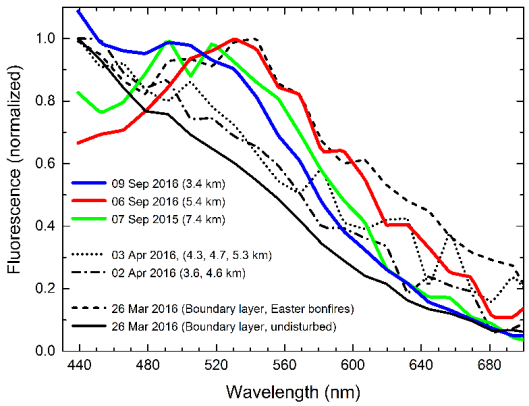

Figure 7: Normalized fluorescence spectra of free-troposphere aerosol. Dates and approximate heights are indicated in the legend. The typical fluorescence spectrum of boundary-layer aerosol as well as the fluorescence spectrum of air laden with biomass-burning aerosol near the ground are shown for comparison.

References

[1] Reichardt, J., 2014: Cloud and aerosol spectroscopy with Raman lidar, *J. Atmos. Ocean. Technol.* **39** (9), 1946-1963.

[2] Reichardt, J., Wandinger, U., Klein, V., Mattis, I., Hilber, B., Begbie, R., 2012: RAMSES: German Meteorological Service autonomous Raman lidar for water vapor, temperature, aerosol, and cloud measurements, *Appl. Opt.* **51** (34), 8111-8131.

[3] Stohl, A., Forster, C., Frank, A., Seibert, P., Wotawa, G., 2005: Technical note: The Lagrangian particle dispersion model FLEXPART version 6.2, *Atmos. Chem. Phys.* **5** (9), 2461-2474.

[4] Yang, P., Liou, K. N., Mishchenko, M. I., Gao, B.-C., 2000: Efficient finite-difference time-domain scheme for light scattering by dielectric particles: application to aerosols, *Appl. Opt.* **39** (21), 3727-3737.